Journal of Structural Geology, Vol. 6, No. 1/2, pp. 201 to 213, 1984
Printed in Great Britain

0191-8141/84 $03.00 + 0.00
Pergamon Press Ltd.

Microstructure and texture in experimentally folded single-layer rock salt

V. K. GAIROLA* and H. KERN

Mineralogisch-Petrographisches Institut Olshausenstr. 40—2300 Kiel, West Germany

(*Accepted in revised form* 30 *June* 1983)

Abstract—Buckling experiments on single-layers of fine-grained artificial polycrystalline rock salt embedded in a plasticine matrix have been performed in the temperature range of 185–200°C under a confining pressure of 10 bars, in a plane strain pure shear apparatus. Strain rates ranged from 2.5×10^{-7} to 4.7×10^{-7}. Layers with an aspect ratio of 7 deformed without buckling, but when this ratio was increased to 13, layers deformed by buckling and produced one wavelength of a sinusoidal fold. The stress–strain and time–strain curves indicate that folding is initiated at about 7 to 8% of bulk deformation. The layer-parallel shortening and thickening continues with progressive folding. The changes in the arclength, thickness, and limb dip show that initially the fold growth is slow, and then becomes rapid.

The inner fold arc is characterized by strong preferred dimensional grain orientation with the longer axis normal to the layer surface. The axial ratio of grains gradually decreases towards the outer arc. The stresses on the outer arc have been relieved mainly by the development of tension fractures. In the limbs, the grains are elongated normal to the layer, however, close to the surfaces the grains are very fine and exhibit a tendency to elongate along the layer surface. The preferred lattice orientation of (100), (110) and (111) planes in halite have been determined by X-ray texture goniometry, and the pole figures are partially comparable to the textures in natural folds from salt domes.

INTRODUCTION

EXTENSIVE theoretical and experimental studies carried out in the past provide useful information on the initiation, mechanics and kinematics of folding. Important contributions on the theories on initiation of buckling in viscous layers have been made by Biot (1961, 1964, 1965) and Ramberg (1961, 1964), and later the theories have been advanced by Chapple (1968, 1969), Sherwin & Chapple (1968) and Fletcher (1974). The progressive shape changes in single-layer folds have been computed by finite element analysis by Dieterich & Carter (1969), Dieterich & Onat (1969) and Shimamoto & Hara (1976). The development of folding has been the topic of experimental investigation for the last two decades. Buckling of single layers has been performed using model materials and the results have been compared with the theoretical models of fold shape geometry and strains (Ghosh 1966, Roberts & Strömgård 1972, Hudleston 1973, Hudleston & Stephansson 1973, Gairola 1977, 1978). Handin *et al.* (1972) have performed folding experiments on single beams of limestone and sandstone under confining pressure and at room temperture, and have discussed the microfractures and analysed the stresses from different parts of the folded layers.

Recently, Wilson (1981) has drawn attention to the importance of the relationship between the intracrystalline processes, the evolution of microstructure and the changes in crystallographic orientations during fold development, and has discussed the fabrics in experimentally folded multilayered ice sheets.

Folding plays a dominant role in the development of salt dome structures. Although halite polycrystals deform at relatively low confining pressures and temperature, no experimental study on rock salt has been done so far. In order to simulate natural conditions of folding, experiments were carried out on single layers of fine-grained rock salt under confining pressure and temperature. The paper describes the fold geometry of the buckled salt layers and discusses the development of the microstructure and texture in the folded layers. The geometrical aspects of the folds are compared with the finite element analysis (Shimamoto & Hara 1976) and experimental results on model materials (Hudlestor 1973, Hudleston & Stephansson 1973, Gairola 1978).

APPARATUS

A shear device was specially made for conducting the experiments. It consists of a cylindrical steel body 10 cm in diameter and 9.5 cm high (Fig. 1a), with two orthogonal boreholes of 4 cm diameter. The axis of one of the boreholes coincides with the axis of the cylinder, and the other borehole passes through the centre of the cylinder (Fig. 1b). The shear apparatus can be separated into two cylindrical halves held together by bolts. This facilitated the removal of the sample after deformation. A heating wire was wound round each half of the cylinder and the temperature was controlled by a transformer. The device can withstand a temperature up to 300°C. The temperature close to the sample was measured by a thermocouple inserted through an aperture in the middle of the box.

Projecting from each end of the boreholes was a piston measuring 5.5 cm in length and 3.98 cm in diameter. The set of pistons parallel to the axis of the cylindrical body was used for compression (σ_1, maximum stress) and the other set confined (σ_3, minimum stress) the

* Present address: Geology Department, Banaras Hindu University, Varanasi-221005, India.

sample. Along the third orthogonal axis (σ_2) there was neither extension nor compression and as such, the test sample remained in nearly plane strain.

The compressive load was achieved by an oil press. A stiff compression spring fixed to a plate situated on either side of the σ_3 axis (Fig. 1a) exerted the confining pressure on the sample through the pistons. A stress of up to 10 bars could be achieved by the springs on the confining pistons. The movement of the pistons was measured by the displacement gauge.

A layer embedded in a cylindrical matrix was inserted in the borehole along the length of the shear apparatus and placed in the middle. On each side along the σ_3 axis, loose powdered matrix material was filled so that along the confining pistons the cylindrical surface of the sample assembly became plane.

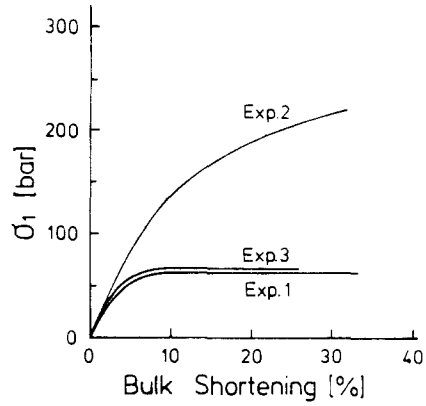

Fig. 2. Stress–strain curves. Exp. 1 and 3 denote the curves for the layers with an aspect ratio of 13.0 and 13.7, respectively, where folding developed. The curve represented by Exp. 2 is for the layer with an aspect ratio of 7.0 which deformed without buckling.

MODEL MATERIAL

Natural rock salt generally occurs in the form of large crystals and is not suitable for making thin layers. Fine-grained (grain size 0.3 mm), artificial rock salt layers were prepared by the method described by Kern & Braun (1973). The width of the layers was 3.98 cm, whereas thicknesses and lengths varied from 0.3 to 0.6 cm, and 4.1 to 4.25 cm, respectively. Layers with an aspect ratio (length/thickness) of 7, 13 and 13.7 were deformed.

Plasticine, which has often been used as a model material, is less stiff than halite and was selected for the matrix. To decrease the viscosity ratio between the layer and matrix, the plasticine was first heated under pressure. Partially dried plasticine was moulded into cylinders of the diameter of 3.98 cm and lengths varying from 4.1 to 4.25 cm, and then cut into two halves along their lengths. Plasticine equal to the thickness of the layer was scraped out from the cut surfaces, and then the layer was sandwiched between these two halves. At a temperature of about 150°C the oil content in the plasticine (Pelikan Nakiplast 680) was partially lost and the dried plasticine exhibited a more or less constant viscosity.

The shear device was insulated after placing the sample in it. The confining springs were then fitted. The temperature was gradually increased at an average rate of 1°C min^{-1}. Because of heat loss and variation in voltage, the temperature could not be precisely controlled and in each experiment it varied from 185 to 200°C. The value for σ_1 was gradually increased so that the pistons moved at the rate of 0.25 mm h^{-1}. Each experiment lasted between 80 and 90 h, however, the deformation rate gradually decreased to a lower value during the night because σ_1 was not maintained.

EXPERIMENTAL RESULTS

The stress–strain curves are presented in Fig. 2. They reveal that for the layer with an aspect ratio of 7, relatively higher stresses are needed as compared with the thin layers having an aspect ratio of 13 or 13.7. The thick layer deformed without folding at a maximum compressive stress of 220 bars on the surface area of the sample, whereas the thinner layers deformed and buckled when the maximum compressive stress reached 60 bars. The stress–strain curves for the thinner layers (Folds 1 & 3) show a quasi-linear behaviour at a constant stress after 7–8% of bulk shortening. This stage was probably reached as soon as buckling initiated. The time–strain curves (Fig. 3), where the time when the stresses decreased to a lower value have been deducted, reveal that initially the strain rate was low and later it became relatively higher. In the noncylindrically folded layers the average strain rate ($\dot{e}$) was 4.7×10^{-7} (Fold 1), whereas in the cylindrically folded layers it was 2.5×10^{-7} (Fold 5). The higher rate of strain in the later stages of deformation probably indicates the initiation of folding, when the fold growth increased. On the basis of finite element analysis, Shimamoto & Hara (1976) have shown that initially the rate of fold growth is slow and it gradually increases up to a certain stage in the deformation history. Thus the time–strain curves support the conclusions drawn from the stress–strain curves that at about 7–8% of bulk shortening, the folding is initiated and then fold growth becomes rapid without further increase in load pressure.

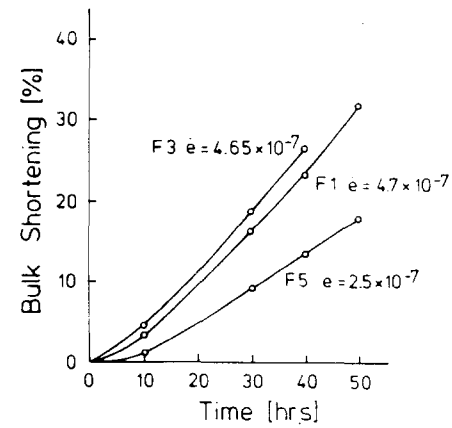

Fig. 3. Time–strain curves for Experiments 1, 3 and 5 (marked F1, F3 and F5). The average strain rate ($\dot{e}$) is indicated for each curve.

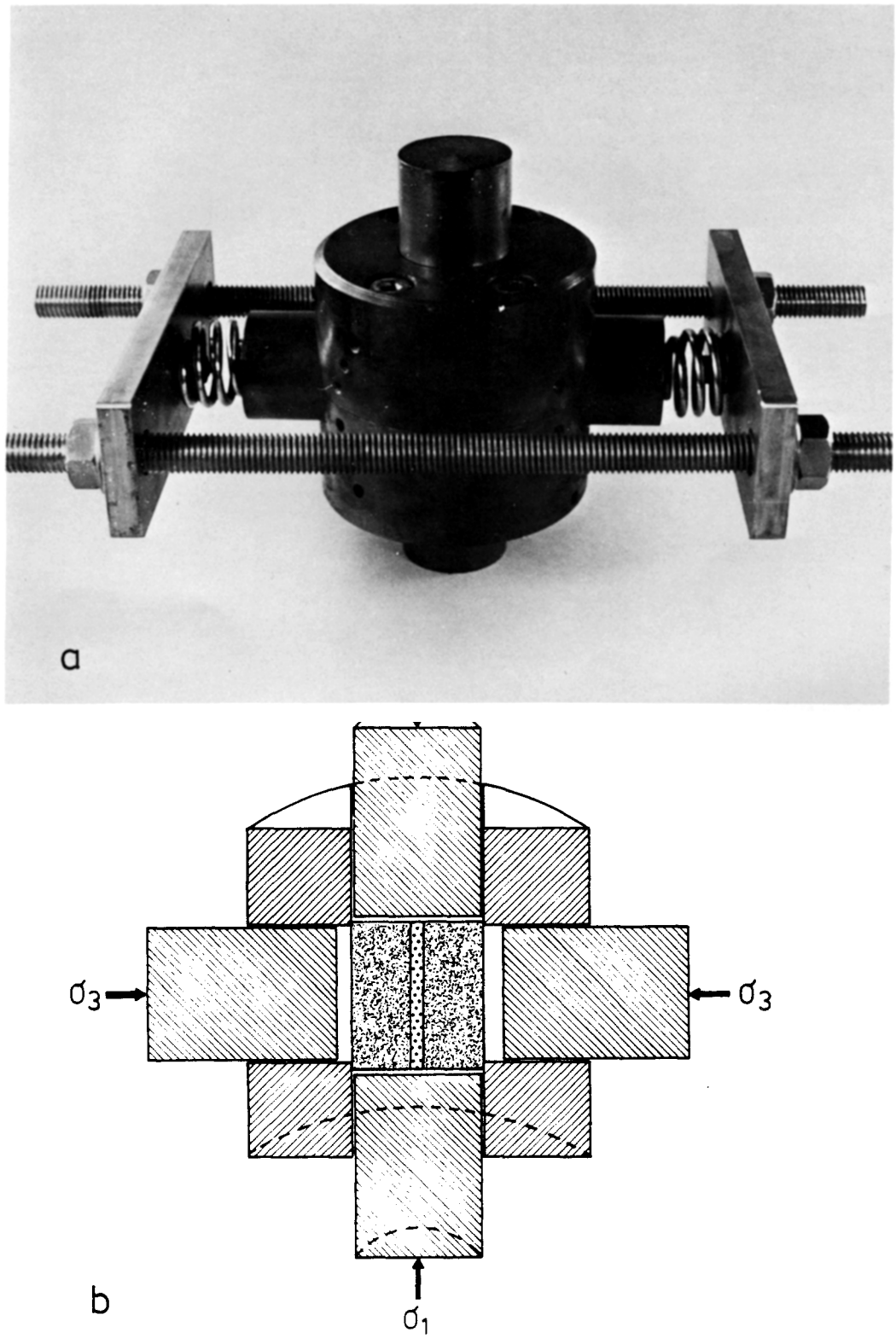

Fig. 1. Plane strain-pure shear apparatus. (a) Photograph showing the set up of the shear device. Compression is achieved through the vertical set of pistons. Springs attached to a plate on either side exert confining pressure through the horizontal set of pistons. Tightening of the nuts on either side of each rod holding the plates increases the confining pressure. (b) Schematic cross-section through the shear device showing sample assemblage in the centre of the cylinder. The compression pistons are denoted by σ_1 and confining pistons by σ_3.

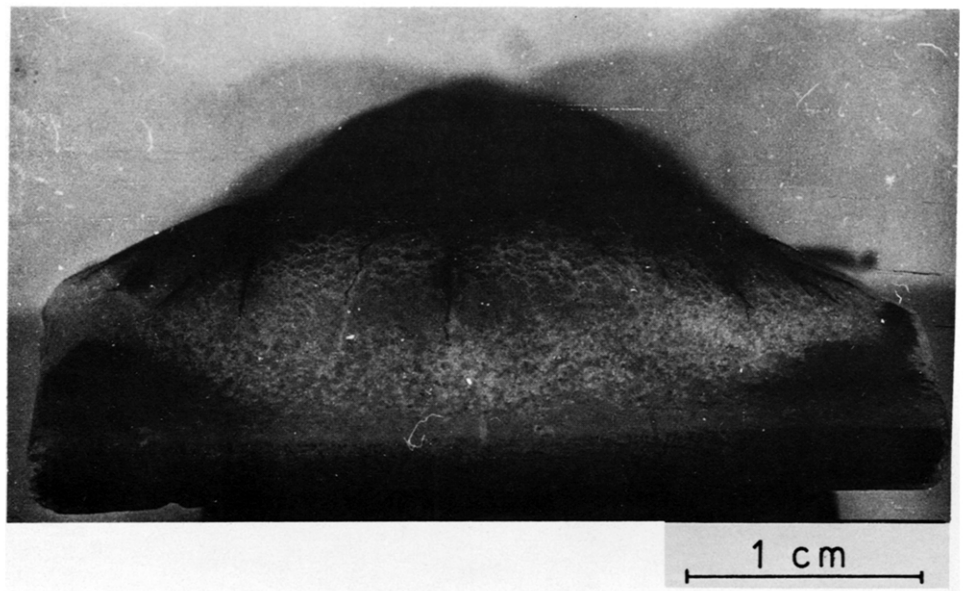

Fig. 4. Plane noncylindrical fold showing tension fractures parallel and perpendicular to the fold hinge direction. Towards the peripheral part of the limb, the fractures are oblique to the hinge.

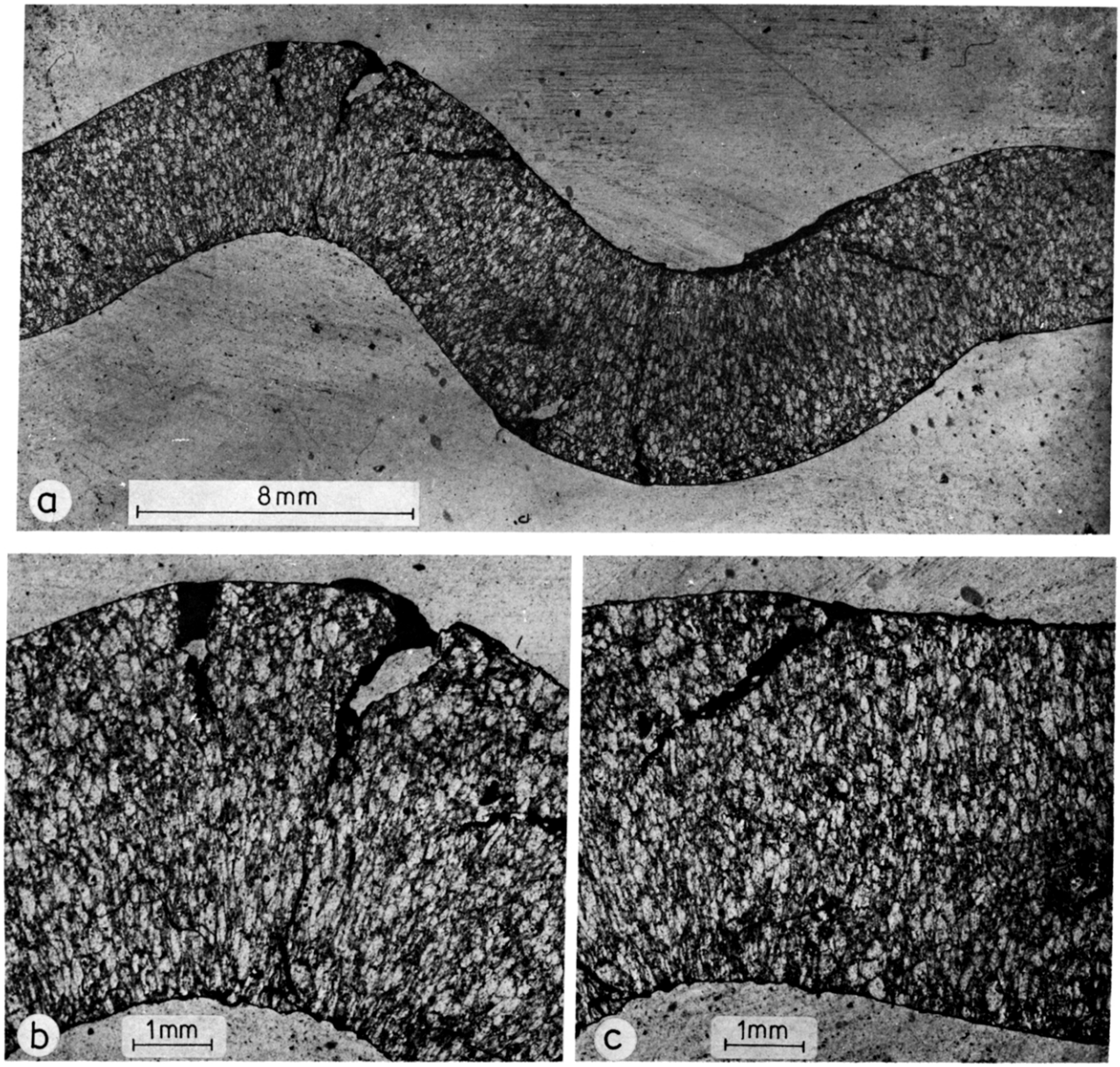

Fig. 7. Photomicrographs showing preferred dimensional grain orientation on the profile section of the folded layer (Fold 1). The outer fold arc is characterized by tension fractures. (a) Folded layer showing one wavelength. (b) Enlargement of fold hinge showing changes in the axial ratio of the grains from the inner arc towards the outer arc, and reduced pore spaces in the inner arc. (c) Enlargement of the limb showing the axial ratio of grains in the layer. Close to the layer surface the grains are smaller in size and exhibit a tendency to elongate along the layer surface.

FOLD SHAPE

The experimental results show that at about 30% bulk shortening, the competent layers with an aspect ratio of 7 underwent layer-parallel shortening and thickening without buckling. However, the layers with an aspect ratio of 13 and above folded (Folds 1, 3 & 5) by buckling after the stage of layer-parallel shortening, and produced one wavelength of the fold (Fig. 7).

Plane noncylindrical folds (Fig. 4) developed in the layers which contained σ_1 and σ_2 axes, whereas plane cylindrical folds resulted in the layers that lay in the plane of the σ_1 and σ_3 axes. In the former type of fold, the hinge showed a culmination. The cylindrical surface of the box normal to the σ_2 axis may have prevented free rotation of the limbs about the fold hinge in the peripheral zone. In the latter type of folds the flat surface of the pistons normal to σ_3 allowed the rotation of the layer.

The buckled layers are characterized by the development of tension fractures on the outer fold arcs (Figs. 4 and 7). The most prominently developed fractures are parallel to the hinge direction (Fig. 4). These fractures are of the tapering type and up to 2 mm deep with a maximum lateral separation of 0.75 mm on the layer surface (Fig. 7). Away from the hinge on the outer arc, the fractures tend to converge towards the inner arc (Fig. 7). In the non-cylindrical folds the fractures are also developed normal to the fold hinge direction because of the culmination and, hence, extension of the fold hinge. At the peripheral part of the fold the second set of tension fractures is oriented obliquely to the hinge direction (Fig. 4). Fractures developed mainly because of the low confining pressure and partly due to the relatively faster strain rate during the later stages of fold development. These fractures may be compared to fractures in naturally folded competent layers deformed at shallow depths.

The data on the mean values of measurements (Table 1) on the profile sections of the buckled layers reveal that the arclength continued to decrease until the maximum bulk shortening (32%) achieved in the experiments. This shows that the layer-parallel shortening is not only restricted to the initial stages of folding. The percentage of decrease in the arclengths is plotted against the bulk shortening (Fig. 5a). It is evident from the graph that the arclength decreases as bulk shortening increases. Further, in the noncylindrical folds the arclength varied on different profile sections of the same fold due to the variation in the amplitude. On the profile section through the culmination point the arclength of the layer is maximum. Thus with a constant wavelength, the amplitude of the fold is also one of the factors which influence the arclength, and hence the layer-parallel shortening.

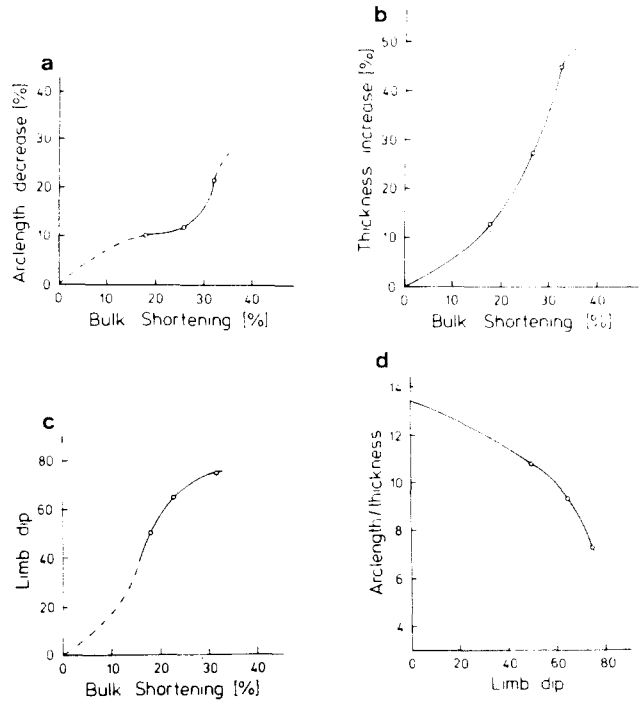

Fig. 5. (a) Changes in arclength with progressive deformation. The part of the curve represented by the solid line is based on data on the folds. This curve has been smoothly extrapolated by a broken line to the point of origin. (b) Changes in layer thickness with progressive deformation. (c) Changes in limb dip (in degrees) with progressive deformation. The part of the curve represented by the solid line is based on data on the folds. This curve has been smoothly extrapolated by a broken line to the point of origin. (d) Changes in the ratio of layer thickness to arclength with limb dip (in degrees).

Table 1. Mean values of measurements on the buckled layers

Fold no.	1	3	5
Original length of the layer (in mm)	42.5	41.1	41.1
Original thickness of the layer (in mm)	3.25	3.0	3.0
Bulk shortening (%)	32.14	26.02	18.66
Arclength (in mm)	33.23	36.1	36.74
Mean hinge thickness (in mm)	4.90	4.05	3.35
Mean limb thickness (in mm)	4.3	3.55	3.25
Amplitude (in mm)	3.42	3.3	3.25
Wavelength (in mm)	18.77	18.0	21.25
Limb dip	75°	65°	50°
Arclength/mean thickness	7.23	9.5	10.8
Fold type	Plane non-cylindrical	Plane non-cylindrical	Plane cylindrical

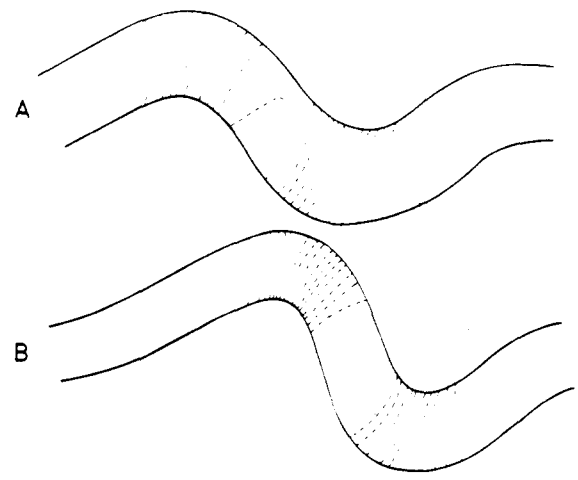

Fig. 6. Dip isogons on the profile section away from the culmination point in Fold 1 (A), and through the culmination point in Fold 3 (B).

From the profile section it can be seen that the fold hinges are thicker than the limbs (Fig. 7, Table 1). In the same layer the thicknesses of two hinges are different, and the limb between two fold hinges is that in the earlier stages of folding the mean percentage of increase in thickness of the fold hinge zone being nearly twice than that in the limbs. With the increase in the bulk shortening, this ratio decreases.

In the experiments previously conducted by Gairola (1978), with plasticine as a layer in putty matrix, the fold hinges continued to thicken, whereas the limbs underwent thinning in the later stages of fold development. The rock salt layers exhibited thickening both in the hinges as well as limbs, with progressive deformation of up to 32%. This amount of deformation was not high enough for thinning of the limbs and, therefore, decrease in the rate of change in thickness. In view of this and as discussed in the following paragraph, in the graph (Fig. 5b) the change in the slope of the curve has been extrapolated by a broken line for further increases in deformation. The overall increase in the thickness with progressive buckling is attributed to the viscosity contrast between the rock salt and dried plasticine.

The overall thickening of the layer is generally attributed to the layer-parallel shortening prior to buckling. The layer-parallel shortening and thickening are a function of the viscosity contrast between the layer and the matrix, and the initial thickness of the layer (Ramberg 1959, Roberts & Strömgård 1972). The experimental results of Hudleston (1973) and Hudleston & Stephansson (1973) supported by the finite element analysis (Shimamoto & Hara 1973), show that the layer-parallel shortening continues until the limbs attain a dip of 20°, and after that it is less significant. The nature of preferred dimensional orientation of the grains (described later) shows that except for the area close to the outer fold arc, the layer in general was subjected to extensive strain perpendicular to the layer surface. This strain geometry resulted in the thickening of the layer. Further, the strains are much higher in the inner fold arcs than the limbs and, therefore, the hinges are thicker than the limbs. In the inner fold arc this strain geometry exists throughout the deformation history and the layer in this zone went on thickening. The thinning of the hinge would be expected only when the extensive strains parallel to the layer surface on the outer fold arc dominate over the effects of strains on the inner arc during the later stages of deformation. In the limbs the thickening reduces with the initiation of layer-parallel shearing (discussed later). With the increase in the amount of layer-parallel shearing a stage may be reached when thinning of the limbs takes place. In the salt layers this stage was not reached mainly because of the low amount of bulk shortening, but also in part because of the low viscosity contrast between the layer and matrix.

Changes in the limb dip with progressive folding have been plotted against the observed bulk shortening, and the curve has been smoothly extrapolated by a broken line up to the point of origin in the graph (Fig. 5c). This graph supports the conclusion drawn from the stress–strain curves (Fig. 2) and time–strain curves (Fig. 3) that initially the fold grows slowly and then rapidly. However, the changes in the limb dip (Fig. 5c) further reveal that after approximately 25% of bulk shortening the rate of fold growth decreased. The decrease in the rate of change of limb dip in the later stages of fold development has also been observed by Hudleston (1973), Hudleston & Stephansson (1973) and Gairola (1978). Compared with the results of Gairola (1978) the rock salt layer shows a rapid fold growth, and the rate of fold growth decreases at an earlier stage of the progressive deformation. On the basis of finite element analysis, Shimamoto & Hara (1976) have suggested that with the decrease in viscosity ratio the fold growth decreases.

The ratios of the arclength and mean thickness of the folded layers are plotted against the limb dip (Fig. 5d). The ratio decreases with the increase in the limb dip, and with progressive folding this ratio decreases rapidly. The observations deviate from the calculations made by Shimamoto & Hara (1976), who showed that after an initial rapid decrease, the rate of change of the ratio (arclength/thickness) is expected to be reduced with progressive folding at a limb dip of 30°. The low viscosity ratio between the layer and the matrix may account for this difference.

The buckled layer is concentric in the fold hinge zones where the arc is circular in shape (Fig. 7). The wavelength/thickness ratio of the noncylindrical folds is 6:1 and in the cylindrical fold it is 7:1. The dip isogons on the profile sections (Fig. 6) reveal that the folds are a combination of Class 1a, 1b and Class 3 type folds of Ramsay (1967). In the outer arc the fold is of Class 1a type which gradually changes to Class 1b type towards the inner arc, and finally has a tendency to belong to Class 3 type at the inner arc.

MICROSTRUCTURE

The fabrics of the experimentally folded rock salt layers exhibit a strong preferred dimensional orientation of halite crystals (Fig. 7). In the inner fold arc zone the grains are intensively elongated normal to the layering. The average ratio of the long to short axes of these grains close to the layer surface is 6:1, and with the increase in deformation, the pore spaces are increasingly reduced. There is variation in this ratio particularly away from the layer surface where it gradually decreases towards the outer arc. Reduction of pore spaces and microcracks is less towards the outer arc, and away from the trace of the axial surface. The preferred dimensional orientation of the grains suggests that the inner fold arc was subjected to compressive strains which gradually decreased towards the outer arc. Close to the layer surface in the outer fold arc, the sense of preferred orientation changes and the grains which are smaller in size, tend to be elongate parallel to the layer surface (Fig. 7). The average ratio of the long to short axes of the grains is 1.25:1. The changeover of the grain orientation on the outer fold arc shows that the layer surface in this zone

underwent tensional strain. The tension fractures on the outer arc (Figs. 4 & 7) also confirm that this part of the fold was subjected to tensional strain parallel to the layering. It is difficult to demarcate the neutral surface separating the compressive strain in the inner fold arc from the tensional strain in the outer arc. However, from the grain orientations it is evident that the neutral surface lies close to the layer surface on the outer fold arc.

The difference in the ratio of long to short axes of the grains in the inner arc to that of the outer arc is mainly due to different deformation paths. The grains in the inner and outer arc zones were initially subjected to compression during layer-parallel shortening prior to buckling, resulting in an incipient grain elongation normal to the layer surface. During the folding stage, compression in the inner arc continued and this zone suffered further compressive strain throughout the deformation. The grains in the outer arc zone were, however, subjected to extension during the folding stage. Thus the effects of compressive strains were superimposed by tensional strain. Part of the tensional strain on the outer arc is compensated by tension fractures, and intragranular deformation is less pronounced. Therefore, the grains in the outer fold arc zone exhibit a low ratio of the long to short axes of the grains. The progressive incremental strains on the inner and outer fold arcs have been discussed by Gairola (1977, 1978), and the results of the present experiments are comparable to the earlier observations.

In the fold limbs the halite grains exhibit preferred dimensional orientation (Fig. 7) throughout the cross-section, except close to the layer surfaces. The longer axis of the grains is oriented perpendicularly to the layer surface. The average ratio of the long to short axes of the grains is 4:1. Grains in the limbs are not as closely packed as in the inner arc fold zone. Close to the layer surface the grains become very fine in size due to cataclasis and show a tendency to preferred dimensional orientation parallel to the layer surfaces (Fig. 7). The higher frequency and larger openings of microcracks in comparison to the inner arc zone are due to rotation of the limbs during the folding stage. The limb zone was thus oblique to the σ_1 and σ_3 axes in the later stages of the deformation history, resulting in shearing of the grains close to the layer surface.

The preferred dimensional orientations of the grains in the folded layers reveal that the fold hinges deformed by tangential longitudinal strain, and the surface area of the limbs were subjected to layer-parallel shearing during the folding stage.

TEXTURE

The fabrics and development of preferred orientation of the poles to crystallographic planes (100), (110) and (111) of halite were investigated by means of a Phillips X-ray texture goniometer with Cu-radiation in reflected mode. Circular plates (11.5 mm diameter) were prepared from slabs cut parallel to the layer surfaces from the inner and outer arcs (Fold 1, 32.1% bulk shortening), and limbs (Fold 1 and Fold 2, 26.8% bulk shortening). It was not possible to investigate the textures of small areas at several locations due to the small dimensions of the folded layers. Further, the folded layers are not thick enough for the verification of pole figures on the planes perpendicular to the fold hinge. The raw intensities of the pole figures were corrected for defocusing by using an undeformed rock salt layer by the method described by Baker *et al.* (1969). Concentrations are represented in multiples of a random distribution (m.r.d.). The pole figures of halite (100), (110) and (111) planes measured on the limbs (Folds 1 & 3) are shown in Fig. 8, the respective diagrams obtained from the inner and outer fold arcs (Fold 1) are presented in Fig. 9. Also shown are the pole figures of the undeformed layer material (Figs. 8a–c), which indicate a random orientation. In all the diagrams the fold hinge direction is indicated by an arrrow (N–S axis, marked '*b*'). '*a*' (E–W axis in the diagrams) denotes the direction on the layer surface perpendicular to the fold hinge, and '*c*' is the axis perpendicular to the layer surface and lies at the centre of the diagrams. In each diagram the orientation of the axial plane has been shown by a broken line. In the diagrams (Fig. 8) for limbs which rotated along the hinge with progressive folding, the σ_2 axis of bulk stress coincides with the '*b*' axis. The axial plane in the diagrams (Fig. 8) contains σ_3, whereas σ_1 is coincident with the pole to the axial plane. In the diagrams (Fig. 9) for the fold hinges the principal bulk stress axes, σ_1, σ_2 and σ_3, coincide with '*a*', '*b*' and '*c*', respectively. On the inner arc the local stresses are coaxial and in the same sense as the bulk stresses, whereas on the outer fold arc the local maximum compressive stress coincides with '*c*', and extensive stress with the '*a*' axis.

Fold limbs

Comparison of the pole figures of the undeformed layer material (having random orientation) with those obtained from folds with moderate (26%) and relatively high (32%) bulk shortening indicates progressive preferred lattice orientation of halite crystals as folding proceeds although the patterns are not significantly pronounced. An interesting feature of all diagrams is that the main maxima are elongated obliquely to the fold hinge direction.

In the less deformed layer (Fig. 8d), the maxima of (100) lie about the '*c*' axis, and there is also a tendency for a weak peripheral girdle. In the more deformed layer (Fig. 8g) the maximum concentration of the poles is found to be sub-parallel to '*c*'.

The poles of the (110) planes in the less deformed layer (Fig. 8e) are distributed over a wider zone about '*c*' with a tendency to elongate along the hinge direction. In the more deformed layer (Fig. 8h) the poles exhibit a maximum concentration on a partially developed small circle girdle around '*c*'. The opening angle of this girdle is about 50°.

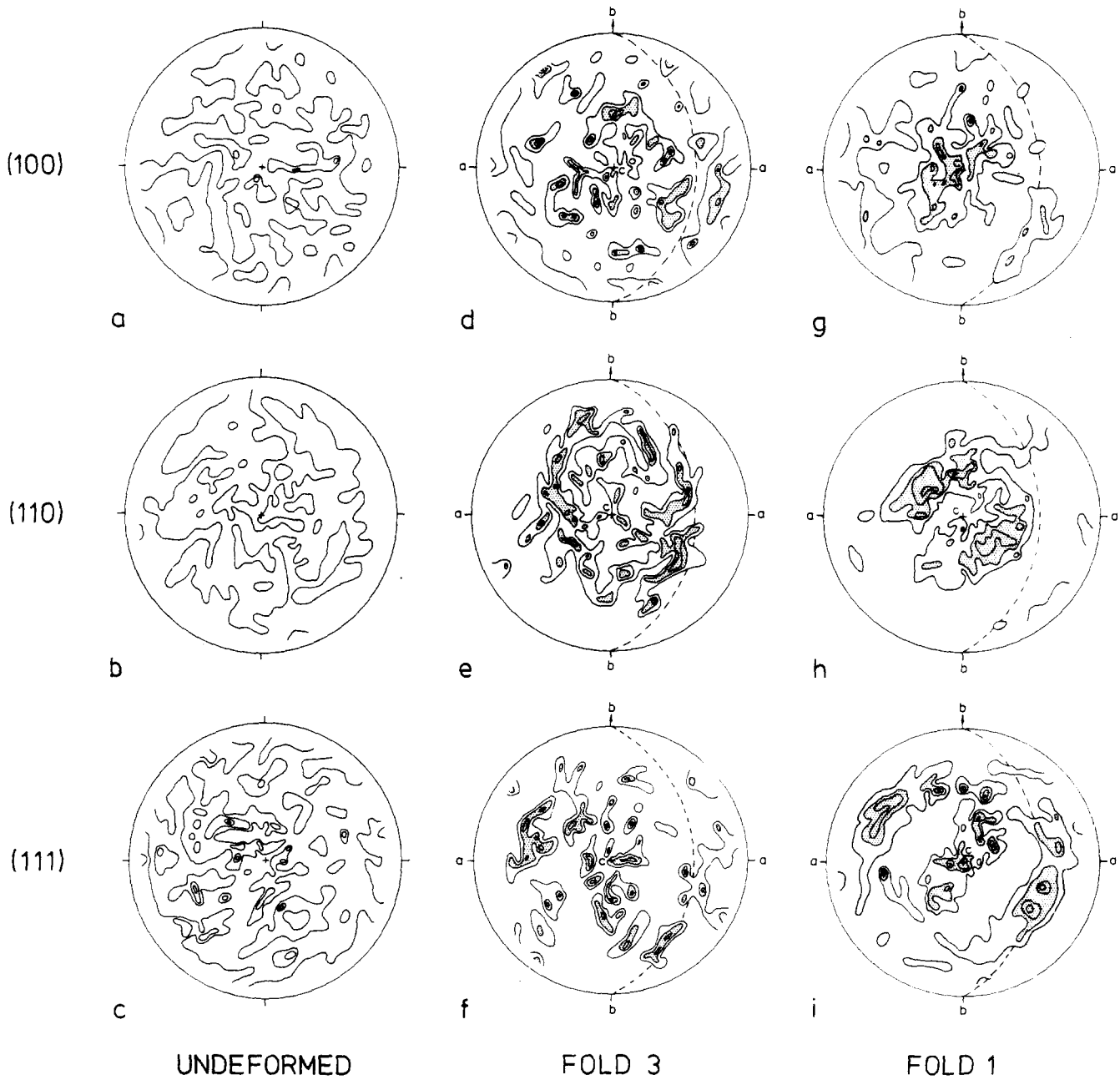

Fig. 8. Pole figures in halite from undeformed layer material and the limbs of Fold 3 (26% bulk shortening) and Fold 1 (32% bulk shortening). Pole intensities for (100) planes (a. d & g). Pole figures for (110) planes (b. e & h). Pole figures for (111) planes (c, f & i). Contour interval: 1.0, 1.3, 1.6 and 2.0% per unit area.

The randomly distributed small maxima of the poles to (111) planes in the less deformed layer (Fig. 8f) exhibit a tendency to elongate in the fold hinge direction. In the more deformed layer (Fig. 8i) the reflected intensities are concentrated in an elongated (N25°E–S25°W direction) central maximum, and a partially developed small circle girdle around '*c*', the opening angle being 110°.

Fold hinges

The pole figures obtained from the fold hinges (Fig. 9) are in general less pronounced than those of the fold limbs (Fig. 8). This is surprising because strong preferred dimensional orientation indicating maximum intragranular strain, was observed in the inner fold arc. The low concentration is probably due to the fact that the strains in the fold hinge are less homogeneous than in the limbs. The pole figures, however, give an overall picture of the reflected intensities of crystals within the area covered by the X-ray beam. A common feature in all the pole figures obtained from the fold hinge zone is that the maxima are more or less symmetrically disposed to the fold hinge direction, and the intensities are in general higher on the inner fold arc than on the outer fold arc.

Inner fold arc

The pole figure for (100) planes (Fig. 9a) exhibits a weak girdle subparallel to the axial plane, and maxima are symmetrically inclined at 30–40° to the axial plane.

In the pole figure of the (110) planes, preferred orien-

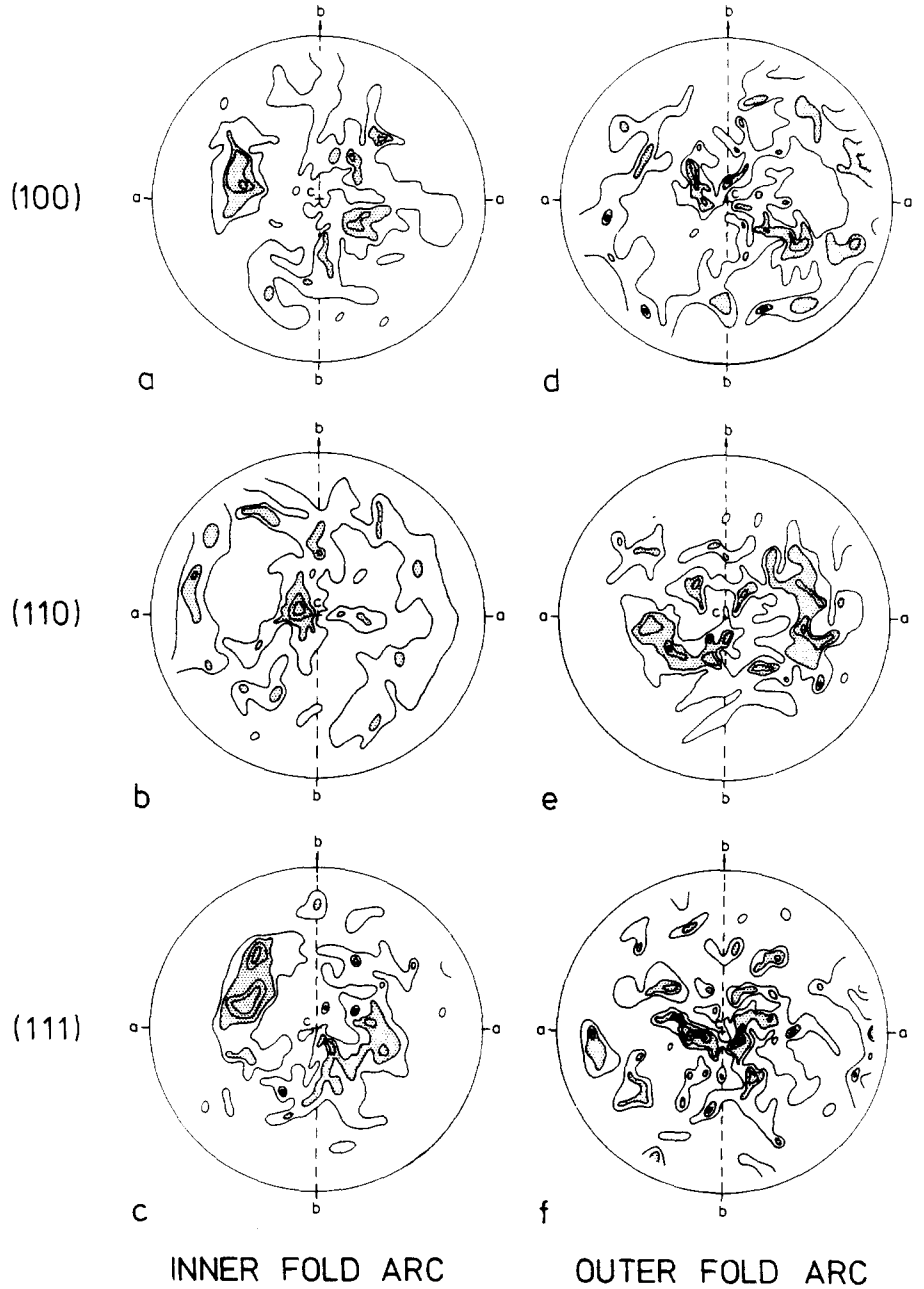

Fig. 9. Pole figures in halite from inner and outer arc zones in Fold 1. Pole figures for (100) planes (a & d). Pole figures for (110) planes (b & e). Pole figures for (111) planes (c & f). Contour interval: 1.0, 1.3, 1.6 and 2.0%.

tation is defined by a central maximum elongated subparallel to the fold hinge direction, and by a partially developed small circle girdle with an opening angle of 120° about the '*c*' axis (Fig. 9b). The pole figure of (111) planes (Fig. 9c) is characterized by a partially developed small circle girdle around '*c*', with an opening angle of about 70°. Further, the girdle has a tendency to elongate in a direction at 25° to the fold hinge.

Outer fold arc

The pole figure of (100) planes (Fig. 9d) exhibits maxima which appear to lie in two small circle girdles around '*c*'. The opening angle of the first girdle is 40° and the second one is 120°. The poles to (110) planes (Fig. 9e) lie around '*c*' in an elliptical shape with the longer axis of the ellipse in the '*a*' direction and the shorter axis in the fold hinge direction. The opening angle along the short axis is 30° and along the long axis it is 80°. The (111) pole figure (Fig. 9f) shows that the maxima have a tendency to scatter in the vicinity of '*c*'.

Discussion

The pole figures of (100), (110) and (111) planes in halite on experimentally deformed cubes of artificial polycrystalline rock salt are characterized by girdles about the principal compressive axis in compression, tensional axis in extension, and intermediate positions between the two axes in plane strain (Kern & Braun 1973). In these experiments, the incremental bulk, as well as local strains, were coaxial throughout the deformation of the homogeneous cubes of rock salt, and the pole figures exhibit well-defined girdles and symmetrical

maxima (Kern & Braun 1973, fig. 5). In principle, the pole figures obtained from the folded rock salt layers (Figs. 8 and 9) may be compared with the pole figures of Kern & Braun (1973), though the intensities are low, small circle girdles are incomplete and/or elliptical in shape, and the maxima are not precisely symmetrical. These anomalies in the pole figures from the folded layers (Figs. 8 and 9) are due to the non-coaxial strains in different parts of the fold (discussed earlier). During folding the limbs were continuously rotating with respect to the bulk strain axes. One hinge which shows a culmination (Fig. 4), was also not coaxial with the bulk strain axes. Therefore, the pole figures have been related to the local strain axes.

In the limb zone, the poles of the planes investigated lie along or in a small circle girdle around '*c*' (Fig. 8), that is the axis normal to the layer surface. The grain orientation (Fig. 7) reveals that this is the direction of tensional strain. It may be stated here that the narrow zone of grain orientation due to layer-parallel shearing was removed during the preparation of the sample for the texture goniometer. In the inner fold arc the local extensive strains are again parallel to the '*c*' axis along and/or around the poles to (110) and (111) planes (Figs. 9b & c). The elliptical nature of the small circle girdles and elongated maxima are due to the triaxial strain and culmination of the hinge. Kern & Braun (1973) have also shown that the patterns of the pole figures differ significantly in uniaxial extension and in triaxial strain. A girdle sub-parallel to the axial plane (Fig. 9a) in the pole figure for the (100) plane is also the effect of triaxial local strain. In the outer fold arc the preferred dimensional orientation of grains (Fig. 7) shows that the zone of layer-parallel extensive strain is very narrow. This zone of tensional strain which gradually reduces towards the neutral surface, was partly removed during the preparation of the sample for the texture goniometer. Thus the indistinct pattern of the pole figures (Figs. 9d–f) reflects the combined effect of strain in the outer and inner fold arcs. Roughly, the poles lie around the '*c*' axis the direction of compressive strain in the outer arc. Kern & Braun (1973) also observed a small circle girdle around the axis of compression.

The fabric diagrams [(100) in halite] in natural folds from Gulf Coast salt domes are characterized by one maximum normal to the axial plane and two maxima on the girdle subparallel to the axial plane (Clabaugh 1962, Muehlberger & Clabaugh 1968). Schwerdtner (1968) observed three maxima that are perpendicular to the axial plane and subparallel as well as subnormal to the lineation, and poorly defined girdles to these maxima. In the experimental folds the pole figures of the (100) planes where poles exhibit maxima close to the axial plane (Fig. 9d), and the girdle is subparallel to the axial plane (Fig. 9a), may be partially compared with the fabric diagrams from the natural folds. The natural isoclinal folds are of the shear type (Muehlberger & Clabaugh 1968) and do not exhibit any preferred dimensional orientation of grains (Carter & Heard 1970) probably as a result of annealing recrystallization. The experimental folds differ from the natural folds and it is not surprising that the fabric diagrams from them are not exactly comparable.

CONCLUSIONS

In the buckling of single layers the aspect ratio is an important factor besides the viscosity ratio, for the development of folds. The stage of layer-parallel shortening prior to buckling is characterized by comparatively lower strain rates and continuous increase in the compressive stresses. During this stage of deformation the competent layer exhibits a lower rate of decrease in the arclength, and increase in the thickness. Once buckling is initiated the strain rate increases and the deformation continues with very small increments in the compressive stresses. The fold growth becomes faster with rapid increase in the limb dip and decrease in the arclength. The thickness of the competent layer continues to increase, and the rate is greater in the hinges than in the limbs. With progressive deformation a stage is reached when the rate of change in the limb dip is retarded and the fold growth decreases.

The decrease in the arclength and increase in thickness which are functions of the aspect ratio of the layer and the viscosity contrast between the layer and matrix, also depend on the wavelength/amplitude ratio. An increase in this ratio reduces the arclength and increases the thickness.

The geometry of the buckle folds changes from the outer arc towards the inner arc from Class 1a to 1b and finally to Class 3 type folds. The preferred dimensional grain orientation reveals that the fold hinge deformed by tangential longitudinal strain. The inner fold arc is subjected to compressive strains throughout the deformation, and as such has a coaxial strain history. The outer fold arc is first subjected to compressive strains, and then to extensile strains during the folding stage. In the fold limbs, the layer-parallel shearing strains are superimposed on the compressive strain produced during the layer-parallel shortening.

Progressive preferred lattice orientation in halite crystals develops with increase in deformation. The limbs exhibit relatively pronounced pole figures compared with fold hinges due to inhomogeneous strains in the latter zones. The pole figures for (100), (110) and (111) planes in halite are in general characterized by maxima and small circle girdles along/or around the axis of extensive strain. The maxima and small circle girdles exhibit a tendency to elongate obliquely to the fold hinge direction. The pole figures from the experimental folds are partly comparable to the fabric diagrams from natural folds in salt domes.

On the basis of relatively weak preferred orientation and relatively large grain size in respect to specific sample areas it is thought that it would be more appropriate if folded layers of larger dimensions having wider homogeneously strained areas, could be used for fabric analysis.

Acknowledgements—The authors are thankful to Dr. A. Richter for his suggestions and taking photomicrographs, and Mr. M. Schroetel for his help in conducting the experiments and preparing the diagrams and photographs. The authors are grateful to Dr. N. J. Price and Dr. J. W. Cosgrove for critically going through the manuscript. Financial assistance from Alexander von Humboldt Stiftung to VKG is gratefully acknowledged.

REFERENCES

Baker, D. W., Wenk, H. R. & Christie, J. M. 1969. X-ray analysis of preferred orientation on fine-grained quartz aggregates. *J. Geol.* **77**, 144–172.

Biot, M. A. 1961. Theory of folding of stratified viscoelastic media and its implications in tectonics and orogenesis. *Bull. geol. Soc. Am.* **72**, 1595–1620.

Biot, M. A. 1964. Theory of viscous buckling of multilayered fluids undergoing finite strain. *Physics Fluids* **7**, 855–861.

Biot, M. A. 1965. Theory of viscous buckling and gravity instability of multilayers with large deformation. *Bull. geol. Soc. Am.* **76**, 371–378.

Clabaugh, P. S. 1962. Petrofabric study of deformed salt. *Science, Wash.* **136**, 193–249.

Carter, N. L. & Heard, H. C. 1970. Temperature and rate dependent deformation of halite. *Am. J. Sci.* **269**, 193–249.

Chapple, W. M. 1968. A mathematical theory of infinite-amplitude rock folding. *Bull. geol. Soc. Am.* **79**, 47–68.

Chapple, W. M. 1969. Fold shape and rheology: the folding of an isolated viscous-plastic layer. *Tectonophysics* **7**, 97–116.

Dieterich, J. H. & Carter, N. L. 1969. Stress history of folding. *Am. J. Sci.* **267**, 129–154.

Dieterich, J. H. & Onat, E. T. 1969. Slow finite deformation of viscous solids. *J. geophys. Res.* **74**, 2081–2088.

Fletcher, R. C. 1974. Wavelength selection in the folding of a single layer with power-law rheology. *Am. J. Sci.* **274**, 1029–1043.

Gairola, V. K. 1977. Three-dimensional strains in fold-hinge zones. *Tectonophysics* **41**, 291–319.

Gairola, V. K. 1978. Strain distribution across an experimental single-layer fold. *Tectonophysics* **44**, 27–41.

Ghosh, S. K. 1966. Experimental tests of buckling folds in relation to strain ellipsoids in simple-shear deformation. *Tectonophysics* **3**, 169–185.

Handin, J., Friedman, M., Logan, J. M., Pattison, L. J. & Swolfs, H. S. 1972. Experimental folding of rocks under confining pressure: buckling of single-layer rock beams. *Mon. Am. geophys. Un.* **16**, 1–28.

Hudleston, P. J. 1973. An analysis of single-layer folds developed experimentally in viscous media. *Tectonophysics* **16**, 189–214.

Hudleston, P. J. & Stephansson, O. 1973. Layer shortening and fold shape development in the buckling of single layers. *Tectonophysics* **17**, 299–321.

Kern, H. & Braun, G. 1973. Deformation und Gefügeregelung von Steinsalz in Temperaturbereich 20–200°C. *Contr. Miner. Petrol.* **40**, 169–181.

Muehlberger, W. R. & Clabaugh, P. S. 1968. Internal structure and petrofabrics of Gulf Coast Salt Domes. *Bull. Am. Ass. Petrol. Geol.* **18**, 1175–1204.

Ramberg, H. 1959. Evolution of ptygmatic folding. *Norsk geol. Tidsskr.* **39**, 99–151.

Ramberg, H. 1961. Contact strain and folding instability of a multilayered body under compression. *Geol. Rdsch.* **51**, 405–439.

Ramberg, H. 1964. Selective buckling of composite layers with contrasted rheological properties, a theory for simultaneous formation of several orders of folds. *Tectonophysics* **1**, 307–341.

Ramsay, J. G. 1967. *Folding and Fracturing of Rocks*. McGraw-Hill, New York.

Roberts, D. & Strömgård, K.-E. 1972. A comparison of natural and experimental strain patterns around fold hinge zones. *Tectonophysics* **14**, 105–120.

Schwerdtner, W. M. 1968. Intergranular gliding in domal salt. *Tectonophysics* **5**, 353–381.

Sherwin, A. A. & Chapple, W. M. 1968. Wavelength of single layer folds: a comparison between theory and observation. *Am. J. Sci.* **266**, 167–179.

Shimamoto, T. & Hara, I. 1976. Geometry and strain distribution of single-layer folds. *Tectonophysics* **30**, 1–34.

Wilson, C. J. L. 1981. Experimental folding and fabric development in multilayered ice. *Tectonophysics* **78**, 139–159.